

HypeVPR: Exploring Hyperbolic Space for Perspective to Equirectangular Visual Place Recognition

Suhan Woo¹ Seongwon Lee² Jinwoo Jang¹ Euntai Kim^{1*}

¹Yonsei University, Korea ²Kookmin University, Korea

wsh112@yonsei.ac.kr sungonce@kookmin.ac.kr 0126jang@yonsei.ac.kr
etkim@yonsei.ac.kr

Abstract

When applying Visual Place Recognition (VPR) to real-world mobile robots and similar applications, perspective-to-equirectangular (P2E) formulation naturally emerges as a suitable approach to accommodate diverse query images captured from various viewpoints. In this paper, we introduce HypeVPR, a novel hierarchical embedding framework in hyperbolic space, designed to address the unique challenges of P2E VPR. The key idea behind HypeVPR is that visual environments captured by panoramic views exhibit inherent hierarchical structures. To leverage this property, we employ hyperbolic space to represent hierarchical feature relationships and preserve distance properties within the feature space. To achieve this, we propose a hierarchical feature aggregation mechanism that organizes local-to-global feature representations within hyperbolic space. Additionally, HypeVPR adopts an efficient coarse-to-fine search strategy, optimally balancing speed and accuracy to ensure robust matching, even between descriptors from different image types. This approach enables HypeVPR to outperform state-of-the-art methods while significantly reducing retrieval time, achieving up to 5× faster retrieval across diverse benchmark datasets. The code and models will be released at <https://github.com/suhan-woo/HypeVPR.git>.

1. Introduction

Visual Place Recognition (VPR) is the task of enabling systems to recognize specific locations across diverse visual environments, playing a crucial role in autonomous navigation [12, 18], augmented reality [32], and scene understanding [20]. Traditional VPR research [3, 7] has primarily focused on perspective-to-perspective (P2P) matching, where both query and database images are perspective images. This approach relies on comparing perspective views using image descriptors. However, P2P matching often re-

quires an extremely large database to accommodate diverse query images captured from various viewpoints, making it impractical for real-world applications.

This limitation underscores the need for perspective-to-equirectangular (P2E) matching. In real-world scenarios, where diverse queries from multiple viewpoints are common, P2E matching leveraging panoramic views offers clear advantages. By encompassing a full 360-degree field of view (FoV), P2E matching inherently improves robustness and efficiency, eliminating the need for an exhaustive, direction-specific database. Given these practical benefits, P2E matching represents a natural evolution in VPR, enabling systems to handle varied queries more flexibly and effectively. However, despite its potential, P2E VPR remains significantly underexplored compared to standard VPR.

Recently, several solutions [35, 41] have been proposed to address the P2E problem. However, existing approaches fail to fully leverage the advantages of equirectangular images. Instead of designing methods tailored to the unique properties of equirectangular images, they primarily adapt and extend P2P solutions to the P2E task using an exhaustive sliding window approach. This results in significant computational inefficiency while overlooking the distinct spatial characteristics of equirectangular images. Moreover, this limitation becomes even more severe as the number of database images increases. To overcome these challenges, a novel approach is required—one that is both computationally efficient and fully exploits the inherent characteristics of equirectangular images.

Our motivation stems from the observation that visual environments are inherently hierarchical [10, 17, 36]. Panoramic views naturally encompass multiple perspective views within their field, and we believe that these relationships can be effectively represented in a hierarchical structure. This insight drives our approach to designing a solution for P2E VPR that leverages this hierarchy, capturing both the broad, global context and essential finer details of the scene in a structured, multi-level framework.

*Corresponding Author.

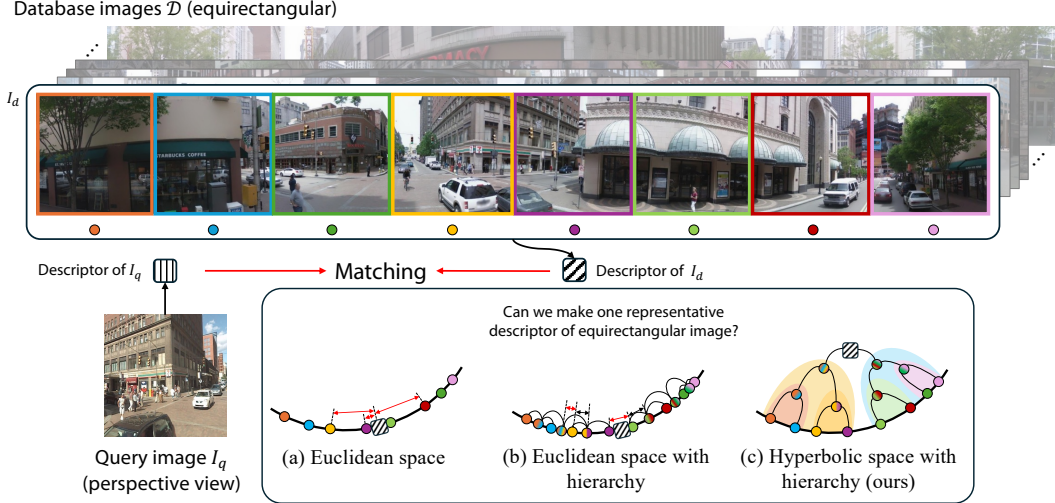


Figure 1. The P2E VPR problem requires matching a distinct query image with a database image, as illustrated. In the example, the yellow-highlighted area (4th from the left) of the database image corresponds to the matching region with the query. However, the non-matching regions vastly outnumber the relevant area, making it challenging to generate a single descriptor for the entire equirectangular image. (a) In Euclidean space, maintaining consistent distances across all regions in a single descriptor is difficult. (b) Even with hierarchical modeling, Euclidean space distorts relational distances, making it difficult to represent hierarchical structures accurately. (c) Our hierarchical modeling, combined with hyperbolic space representation learning, enables a single descriptor that effectively captures all regions. Moreover, using geodesic distances in hyperbolic space instead of Euclidean distances allows for more robust matching across different FoVs.

In this paper, we introduce HypeVPR, a novel approach to VPR that leverages the strengths of hyperbolic space for P2E matching. HypeVPR fully exploits the ability of hyperbolic space to represent hierarchical structures within a non-linear distance space [11, 17, 22], as illustrated in Figure 1. This property allows hyperbolic space to model hierarchical structures with minimal distortion [38, 39] and ensures robust matching even between descriptors with differing FoVs. Leveraging this characteristic, HypeVPR segments panoramic views into regions with varying FoVs and organizes these features hierarchically in the embedding space: higher levels capture broad contextual information, while lower levels focus on finer, localized scene details. This hierarchical structuring supports a multi-scale, coarse-to-fine search strategy, where broad candidate locations are rapidly identified at higher levels, followed by precise matching at progressively finer levels. Furthermore, this framework provides a flexible trade-off between retrieval speed and accuracy without additional training, making it adaptable to various application needs. By effectively balancing panoramic coverage and localized detail, this layered approach establishes HypeVPR as a robust and efficient solution for P2E VPR tasks that require both comprehensive and precise visual matching.

Through extensive experiments, we demonstrate that HypeVPR achieves superior performance across various benchmarks while significantly improving retrieval efficiency. Compared to existing methods, it offers not only better accuracy but also substantially faster retrieval and re-

duced descriptor storage requirements. Our contributions can be summarized as follows:

- We introduce HypeVPR, a hyperbolic space-based VPR framework specifically designed for efficient P2E matching, marking the first approach to tackle P2E VPR without relying on sliding window techniques.
- We propose a hierarchical embedding and training scheme for HypeVPR that effectively models the relationships between equirectangular and perspective views.
- We incorporate an efficient coarse-to-fine strategy within the hierarchical embedding framework, specifically designed for the reranking process by effectively balancing retrieval speed and accuracy.
- With the aforementioned contributions, we achieve new state-of-the-art performance on the YQ360 [41] and Pitts250K-P2E [41] datasets.

2. Related Works

Visual place recognition. Recent VPR models [2, 19, 21, 31, 40, 43, 46] focus on P2P matching between query and database images. However, this approach requires extensive databases containing images captured from all possible query directions at the same location, which is impractical for real-world scenarios. To address this, equirectangular-to-equirectangular VPR methods [9, 14, 44] have been proposed, but they rely on specialized cameras to capture equirectangular query images, further limiting their prac-

tality. Consequently, the P2E VPR [35, 41] approach emerges as a more practical alternative, though research in this area remains in its early stages. Orhan *et al.* [35] and Ze *et al.* [41] addressed the FoV mismatch between query and database images by adapting the traditional matching method with a sliding window approach. However, these methods remain computationally expensive due to the need for comparisons across multiple windows in equirectangular images, highlighting the need for a novel approach tailored to P2E scenarios. In this work, we present HypeVPR, a novel method that surpasses traditional P2E approaches by leveraging hierarchical embeddings in hyperbolic space. Unlike the time-consuming sliding window techniques, HypeVPR captures both global and local details in a single, multi-level descriptor, enabling efficient, coarse-to-fine matching across the full 360-degree view. This approach enhances search speed, reduces memory requirements, and sets a new standard for accurate and robust P2E VPR.

Hyperbolic space. Embeddings in hyperbolic space have gained significant attention for effectively modeling hierarchical structures. Hyperbolic spaces are naturally suited to embed hierarchies (e.g., tree graphs) with low distortion [38, 39]. In NLP, they have enabled breakthroughs in mapping the hierarchical nature of language [33, 34]. This success has spurred applications in computer vision, with notable advances in representation learning [17], image retrieval [13, 23], image segmentation [4, 45], few-shot learning [16], and image generation [28]. Pioneering work by Khrulkov *et al.* [22] showed that embedding images in hyperbolic space is more effective than in Euclidean space, especially for data with hierarchical structures. Desai *et al.* [11] extended this to multi-modal datasets, and Kwon *et al.* [27] utilized hyperbolic embeddings to improve the hierarchical understanding of visual scenes in pre-trained networks. In this work, we leverage the hyperbolic space to embed hierarchical structures within equirectangular images, enhancing robustness in visual place recognition across varying fields of view. By capturing both global panoramic context and essential local details in a unified hyperbolic embedding, our approach provides a powerful representation that is resilient to FoV variations, setting a new standard for accuracy and efficiency in P2E VPR.

3. Preliminaries

3.1. Hyperbolic geometry

Formally, an n -dimensional hyperbolic space, denoted as \mathbb{H}^n , is defined as a homogeneous, simply connected n -dimensional Riemannian manifold with constant negative sectional curvature. This property of negative curvature gives hyperbolic space similarities to the Euclidean sphere, even though it cannot be isometrically embedded in Euclidean space [25, 29]. Nevertheless, five well-studied models of hyperbolic geometry exist, each equipping a subset

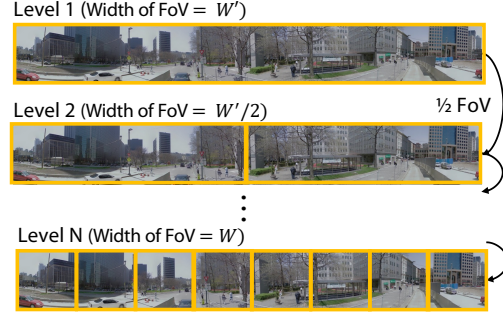


Figure 2. Hierarchical modeling of equirectangular image.

of Euclidean space with a hyperbolic metric. These models are isomorphic, enabling transformations between them based on the formulas of interest. For HypeVPR, we selected the Poincaré ball model, as it is the most extensively studied [15, 17, 22, 28, 33].

Poincaré ball model. The Poincaré ball model $(\mathbb{D}^n, g^{\mathbb{D}})$ is defined by the manifold $\mathbb{D}^n = \{\mathbf{x} \in \mathbb{R}^n : \|\mathbf{x}\| < 1\}$ equipped with the *Riemannian metric* $g_{\mathbf{x}}^{\mathbb{D}} = \lambda_{\mathbf{x}}^{c^2} g^E$, where

$$\lambda_{\mathbf{x}}^c := \frac{2}{1 - c\|\mathbf{x}\|^2} \quad (1)$$

is the conformal factor and g^E is the Euclidean metric tensor $g^E = I^n$. In this model, the *geodesic distance* between two points is given by the following expression:

$$d_{\mathbb{D}}(\mathbf{x}, \mathbf{y}) = \operatorname{arccosh} \left(1 + 2 \frac{\|\mathbf{x} - \mathbf{y}\|^2}{(1 - \|\mathbf{x}\|^2)(1 - \|\mathbf{y}\|^2)} \right). \quad (2)$$

3.2. Hyperbolic operations

We use the generalized formula for operation on the Poincaré ball with an additional curvature parameter c , which modifies the ball’s curvature, following [15, 22].

Distance. The induced distance function from equation (2) with curvature c in Poincaré ball is defined as

$$d_c(\mathbf{x}, \mathbf{y}) := \frac{2}{\sqrt{c}} \operatorname{arctanh}(\sqrt{c}\|\mathbf{x} \oplus_c \mathbf{y}\|), \quad (3)$$

where \oplus_c is Möbius addition with curvature c .

Exponential and logarithmic maps. To perform operations within hyperbolic space, it is essential to establish a bijective mapping from \mathbb{R}^n to \mathbb{D}_c^n , allowing for the conversion of Euclidean vectors into hyperbolic space coordinates, and vice versa. The exponential and logarithmic maps provide this bijection, with the former mapping Euclidean vectors to hyperbolic space and the latter serving as its inverse.

The *exponential* map $\exp_{\mathbf{x}}^c$ is a function from tangent space $T_{\mathbf{x}}\mathbb{D}_c^n \cong \mathbb{R}^n$ to \mathbb{D}_c^n , defined as

$$\exp_{\mathbf{x}}^c(\mathbf{v}) := \mathbf{x} \oplus_c \left(\tanh \left(\frac{\sqrt{c}\lambda_{\mathbf{x}}^c\|\mathbf{v}\|}{2} \right) \frac{\mathbf{v}}{\sqrt{c}\|\mathbf{v}\|} \right). \quad (4)$$

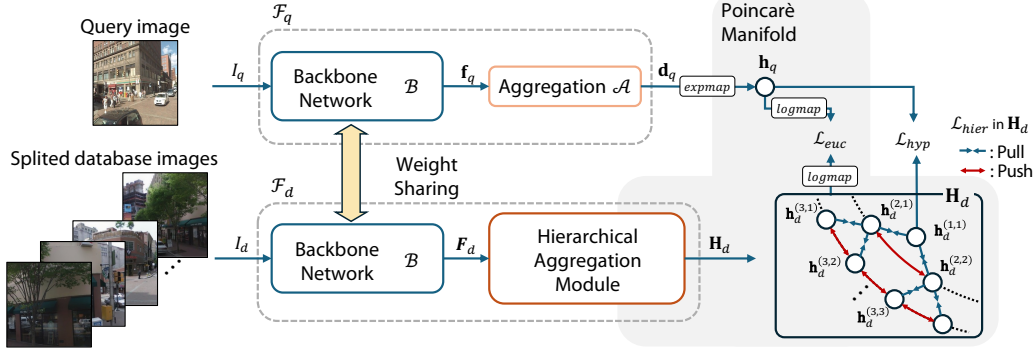


Figure 3. Structure of our network and our training scheme.

The inverse *logarithmic* map is defined as

$$\log_{\mathbf{x}}^c(\mathbf{y}) := \frac{2}{\sqrt{c}\lambda_{\mathbf{x}}^c} \operatorname{arctanh}(\sqrt{c}\|\mathbf{x} \oplus_c \mathbf{y}\|) \frac{-\mathbf{x} \oplus_c \mathbf{y}}{\|\mathbf{x} \oplus_c \mathbf{y}\|}. \quad (5)$$

In practice, the maps \exp_0^c and \log_0^c are utilized to transition between Euclidean and Poincaré ball representations of a vector.

4. Method

In this section, we propose HypeVPR, a P2E Visual Place Recognition Network leveraging hyperbolic space. The key aspect of HypeVPR is its ability to output visual descriptors from equirectangular images that can be directly compared with those from perspective view (PV) images.

4.1. Overview

Our framework builds upon the traditional VPR structure. Given a query image with an unknown location $I_q \in \mathbb{R}^{H \times W \times C}$ and a large set of M geotagged database images $I_d \in \mathcal{D} \subset \mathbb{R}^{H \times W' \times C}$ ($W' > W$), our goal is to identify the top-ranked database images that can serve as potential location suggestions for the query. This is typically achieved by designing a network \mathcal{F} , which acts as an image representation extractor, producing a fixed-size vector $\mathbf{d} = \mathcal{F}(I) \in \mathbb{R}^{C_d}$ for a given image I . For the database images, this feature extraction can be performed offline, while for the query image, it is done online. At test time, these fixed-size vectors, referred to as descriptors, are compared using distance metrics, and the database images are ranked based on their proximity to the query.

In HypeVPR, to match descriptors from the perspective query I_q with the corresponding equirectangular database image I_d despite FoV differences, we hierarchically model the equirectangular database images and embed their features in hyperbolic space. Hyperbolic space naturally captures hierarchical structures through its exponential distance scaling, enabling fine-grained local features and global panoramic contexts to be effectively represented. Its unique

geometric properties preserve proximity between descriptors across varying FoVs while separating those from different scenes, enhancing the robustness of VPR. To further reinforce these properties, the proposed hyperbolic aggregation method and training scheme are designed to effectively capture and maintain these relationships. Additionally, the hierarchical modeling naturally facilitates a coarse-to-fine reranking mechanism for precise descriptor matching.

4.2. Hierarchical modeling of equirectangular image

For hierarchical modeling of the equirectangular image, we progressively break down the equirectangular image I_d into smaller images through multiple levels. Specifically, when we are given a database image I_d with a width of W' , we put it at the top level of the hierarchy by $I_d^{(1)} = I_d$ and progressively halve the width to create the subsequent levels, as illustrated in Figure 2. Thus, the size of the image $I_d^{(\ell)}$ corresponding to level ℓ is given by

$$I_d^{(\ell)} \in \mathbb{R}^{H \times \frac{W'}{2^{\ell-1}} \times C}. \quad (6)$$

In our implementation, when the depth of the hierarchy is L , that is, when $\ell = 1, \dots, L$, we resize I_q and I_d into a square image of size $W \times W$ and a long horizontal image of size $W \times (2^{L-1} \cdot W)$, respectively, so that the query image I_q and the database sub-image $I_d^{(L)}$ at the bottom level L can have the same size and share a backbone network.

4.3. Network design

Traditional VPR methods typically use the same network for both query and database images due to their similar shapes. In contrast, P2E VPR presents unique challenges arising from differing image formats. Processing entire high-resolution equirectangular images at once incurs significant computational costs.

To address these issues and leverage the well-established strengths of P2P architectures in stable descriptor matching, we employ a unified input size and shared backbone for both query and database images. Specifically, database

images are divided to match the query image size (corresponding to the lowest tree level) and passed through the backbone to extract features. These features are then hierarchically aggregated in a bottom-up manner, forming an L -level hierarchical tree structure.

4.4. Network for Query Descriptors

The network \mathcal{F}_q on the first path of Figure 3 aims to generate a query descriptor from a query image I_q and consists of two components: The first component is the backbone network \mathcal{B} , which extracts the feature representation \mathbf{f} . The second component is the aggregator \mathcal{A} , which transforms \mathbf{f} into the final descriptor \mathbf{d} . Given an input query image I_q , the network generates the Euclidean query image descriptor \mathbf{d}_q as follows:

$$\mathbf{d}_q = \mathcal{F}_q(I_q) = \mathcal{A}(\mathcal{B}(I_q)). \quad (7)$$

The feature extraction operation is expressed as $\mathbf{f}_q = \mathcal{B}(I_q)$. For aggregation, we use GeM pooling [37], which can pool various types of information depending on the parameter p :

$$\mathbf{d}_q = \mathcal{A}(\mathbf{f}_q) = \text{GeM}(\mathbf{f}_q) = \left(\frac{1}{|\mathbf{f}_q|} \sum_i f_{q,i}^p \right)^{\frac{1}{p}}, \quad (8)$$

where f_i is the i -th element of \mathbf{f} .

To embed the Euclidean space descriptor \mathbf{d}_q into the hyperbolic descriptor embedding \mathbf{h}_q , we use Equation (4) as follows:

$$\mathbf{h}_q = \exp_0^c(\mathbf{d}_q) = \tanh(\sqrt{c}\|\mathbf{d}_q\|) \frac{\mathbf{d}_q}{\sqrt{c}\|\mathbf{d}_q\|}. \quad (9)$$

This hyperbolic descriptor \mathbf{h}_q is used for matching with the database descriptors.

4.5. Hierarchical aggregation network for database descriptors

The network \mathcal{F}_d on the second path of Figure 3 is designed to generate a descriptor \mathbf{H}_d from a database image I_d . A key challenge in designing the database network is that it must generate an efficient database descriptor \mathbf{H}_d : one that is the same size as the query descriptor \mathbf{h}_q but contains significantly more information. To address this, we designed a new aggregation module for the descriptor network \mathcal{F}_d , called the hierarchical aggregation module (HAM).

Since \mathcal{F}_q and \mathcal{F}_d share the same backbone \mathcal{B} , the output from the network \mathcal{F}_d is represented by

$$\mathbf{H}_d = \mathcal{F}_d(I_d) = \text{HAM}(\mathcal{B}(I_d)). \quad (10)$$

As we mentioned, first we divide database image I_d into 2^{L-1} windows for the L -th level. $I_d^{(L)} = \{w^j : j = 1, \dots, 2^{L-1}\}$ and extract feature from each window by

$$\mathbf{F}_d = \{\mathbf{f}_d^j = \mathcal{B}(w^j) : w^j \in I_d\}. \quad (11)$$

To generate an descriptor \mathbf{H}_d which represent whole panoramic image, we aggregate these window-based features \mathbf{f}_d^j using HAM.

Hierarchical aggregation module (HAM). The purpose of HAM is to aggregate Euclidean features and generate hierarchical features in hyperbolic space with L levels. First, we apply level-wise GeM pooling to \mathbf{F}_d to obtain the level-wise Euclidean descriptors $\mathbf{d}_d^{(\ell),j}$, given by:

$$\mathbf{d}_d^{(\ell),j} = \text{GeM}_\ell(\mathbf{f}_d^j). \quad (12)$$

GeM has a parameter p_ℓ for each level, allowing the network to aggregate features appropriately at different levels of the tree. We then project each descriptor $\mathbf{d}_d^{(\ell),j}$ into hyperbolic space:

$$h_d^{(\ell),j} = \exp_0^c(\mathbf{d}_d^{(\ell),j}). \quad (13)$$

At level ℓ , we partition $h_d^{(\ell),j}$ into $2^{\ell-1}$ non-overlapping groups $h_d^{(\ell,k)}$ as in Figure 2 to form $\mathbf{H}_d^{(\ell)}$ using a hyperbolic aggregation function \mathcal{A}_H :

$$\mathbf{H}_d^{(\ell)} = \{\mathbf{h}_d^{(\ell,k)} = \mathcal{A}_H(\{h_d^{(\ell),j} : j \in \mathcal{I}_d^{(\ell,k)}\})\}. \quad (14)$$

where the index set for the k -th group at level ℓ is defined as:

$$\mathcal{I}_d^{(\ell,k)} = \{j \mid (k-1) \cdot 2^{L-\ell} + 1 \leq j \leq k \cdot 2^{L-\ell}\}, \quad (15)$$

where L is the total number of levels, ℓ is the current level, and k ranges from 1 to $2^{\ell-1}$.

We use hyperbolic averaging [22] as the hyperbolic aggregation function \mathcal{A}_H . In [22], the *Klein model* of hyperbolic space, which has geodesics represented as straight lines, is used to define the *hyperbolic average*. They extend the averaging operation to hyperbolic space using the *Einstein midpoint*, which takes its simplest form in *Klein* coordinates (see Section S2 for details). We use same operation for our hyperbolic aggregation function:

$$\mathcal{A}_H(h_d^{(\ell),1}, \dots, h_d^{(\ell),2^{L-\ell}}) = \frac{\sum_{j=1}^{2^{L-\ell}} \gamma_j h_d^{(\ell),j}}{\sum_{j=1}^{2^{L-\ell}} \gamma_j}, \quad (16)$$

where γ_i are known as the Lorentz factors defined as:

$$\gamma_j = \frac{1}{\sqrt{1 - c\|h_d^{(\ell),j}\|^2}}. \quad (17)$$

The Lorentz factor reflects the hyperbolic geometry where distances increase as points move farther from the origin, enabling accurate averaging in the correct direction.

We denote the set of all hyperbolic hierarchical features $\mathbf{h}_d^{(\ell,k)}$ across all levels ℓ and nodes k as \mathbf{H}_d . To ensure \mathbf{H}_d

maintains a hierarchical structure and enables robust matching between query and database descriptors, it is trained using the loss introduced in Section 4.7. We use $\mathbf{h}_d^{(1,1)}$ as the representative descriptor of the database image, which is directly compared with the query descriptor.

The figure of HAM is provided in the supplementary material (Figure S4).

4.6. Reranking in hierarchy

Even when using hyperbolic space, handling all possible angles of a query image in a 360-degree setting by only one descriptor remains challenging. To address this, we propose a novel hierarchical reranking process.

During our training, the hierarchical structure of the database descriptors naturally enables flexible representation during descriptor matching, similar to Matryoshka representation [26]. Rather than using only the highest-level descriptor for matching, we can flexibly select lower-level descriptors, allowing for an adjustable trade-off between computation time and accuracy.

To make an initial prediction, we compare the query descriptor with the first-level descriptors of the database using the hyperbolic distance from Equation (3). We then retrieve the top K' ($K' > K$) nearest neighbors and perform reranking to obtain the final top K predictions. For reranking, we select a desired set of levels from the remaining $L-1$ levels, excluding the first level, to refine the prediction.

To express the hyperbolic distance at each level as a normalized score, we define the score at level ℓ with scaling factor γ as follows:

$$s_\ell = \max_k \exp \left\{ -\frac{1}{\gamma} d_c(\mathbf{h}_q, \mathbf{h}_d^{(\ell,k)}) \right\}. \quad (18)$$

Using the initial score s_1 and the score s_ℓ from the selected level set $\mathbb{L} \subset \{2, \dots, L\}$, we compute the final score as:

$$s = w_1 s_1 + \sum_{\mathbb{L}} w_\ell s_\ell. \quad (19)$$

The final top K prediction is obtained by reranking the H initial predictions based on the final score s . Adjusting \mathbb{L} enables a flexible trade-off between retrieval speed and accuracy without additional training.

4.7. Training objectives

We train the descriptors in both Euclidean and hyperbolic spaces using three different loss functions based on the triplet loss [5].

Hierarchical triplet loss. To learn the hierarchical tree structure of \mathbf{H}_d , we modify the hierarchical contrastive loss proposed in [27] and further refine it into a triplet loss, explicitly ensuring that descriptors with overlapping FoVs across subsequent levels are pulled closer, while those at the

same level but from different regions are pushed apart, as illustrated in Figure 3. The modified loss is formulated using the distance metric d_c in Equation (3) as follows:

$$\mathcal{L}_{\text{hier}} = \sum_{\mathbf{H}_d} \max \left\{ d_c \left(\mathbf{h}_d^{(\ell-1,k)}, \mathbf{h}_d^{(\ell,2k-b)} \right) - d_c \left(\mathbf{h}_d^{(\ell,2k-b)}, \mathbf{h}_d^{(\ell,n)} \right) + m, 0 \right\}. \quad (20)$$

Here, ℓ ranges from 2 to L , representing the hierarchical levels of the feature pyramid. The index b takes values $\{0, 1\}$, while n iterates over all other samples at level ℓ , excluding $n = 2k - b$, as negatives. m represents the margin of the triplet loss.

Hyperbolic triplet loss. We use \mathcal{L}_{hyp} for matching the representative descriptor $\mathbf{h}_d^{(1,1)}$ of \mathbf{H}_d and the query descriptor \mathbf{h}_q . \mathcal{L}_{hyp} is defined using distance metric d_c as follows:

$$\mathcal{L}_{\text{hyp}} = \sum \max \left\{ d_c \left(\mathbf{h}_q, \mathbf{h}_{d,\mathbb{P}}^{(1,1)} \right) - d_c \left(\mathbf{h}_q, \mathbf{h}_{d,\mathbb{N}}^{(1,1)} \right) + m, 0 \right\}, \quad (21)$$

where \mathbb{P}' and \mathbb{N}' denote the positive and negative samples selected from the sets \mathbb{P} and \mathbb{N} , respectively, using the mining method described in [41]. The sets \mathbb{P} and \mathbb{N} are determined before training.

Euclidean triplet loss. Since training in hyperbolic space is unstable, guidance in Euclidean space is necessary. Additionally, the window-based features must be well-learned to ensure the proper generation of features at other levels. Therefore, we apply the window-based Euclidean triplet loss \mathcal{L}_{euc} to train the query descriptor and the L -th (lowest) level of the database descriptor in Euclidean space using the L_2 distance. To achieve this, we first map the hyperbolic descriptors \mathbf{h}_q and $\mathbf{H}_d^{(L)}$ back to Euclidean space using Equation (5), and then apply \mathcal{L}_{euc} to the resulting Euclidean descriptors \mathbf{d}_q and $\mathbf{D}_d^{(L)}$.

$$\mathcal{L}_{\text{euc}} = \sum \max \left\{ \|\mathbf{d}_q - \mathbf{d}_{d,\mathbb{P}'}^{(L)}\|_2 - \|\mathbf{d}_q - \mathbf{d}_{d,\mathbb{N}'}^{(L)}\|_2 + m, 0 \right\}. \quad (22)$$

\mathbb{P} and \mathbb{N} are the same sets used in \mathcal{L}_{hyp} .

Overall objectives. The overall objectives are defined as:

$$\mathcal{L} = \mathcal{L}_{\text{hier}} + \mathcal{L}_{\text{hyp}} + \mathcal{L}_{\text{euc}}. \quad (23)$$

5. Experiments

In this section, we conduct extensive experiments to demonstrate the effectiveness of our proposed HypeVPR for the P2E VPR task.

Method	#Params.	Time/q	R@1	R@5	R@10	R@20
NetVLAD [3]	7.23	0.7	35.2	66.8	80.0	90.8
Berton <i>et al.</i> [7]	86.86	0.7	40.4	74.8	88.4	95.8
Orhan <i>et al.</i> [35]	136.62	5734.4	47.6*	79.2*	88.4*	95.2*
PanoVPR (SwinT) _{×8} [41]	28.29	4.9	30.8	69.6	81.6	92.4
Ours -R (SwinT) _{×8}	28.29	0.7	30.8	65.6	78.0	90.8
Ours (SwinT) _{×8}	28.29	4.0	32.0	69.6	84.4	90.8
PanoVPR (SwinT) _{×16} [41]	28.29	11.0	43.2	82.4	90.8	96.4
Ours -R (SwinT) _{×16}	28.29	0.7	37.6	68.0	80.4	91.6
Ours (SwinT) _{×16}	28.29	6.7	45.6	84.0	91.2	96.4
PanoVPR (ConvNeXtS) _{×8} [41]	50.22	4.9	39.6	76.8	87.6	94.0
Ours -R (ConvNeXtS) _{×8}	50.22	0.7	35.2	68.0	80.4	92.8
Ours (ConvNeXtS) _{×8}	50.22	4.0	43.8	78.8	89.2	96.0
PanoVPR (ConvNeXtS) _{×16} [41]	50.22	11.0	46.0	83.2	92.4	97.2
Ours -R (ConvNeXtS) _{×16}	50.22	0.7	43.2	81.2	91.6	98.4
Ours (ConvNeXtS) _{×16}	50.22	6.7	52.4	85.2	94.8	98.0

(a) Performance on the YQ360 dataset.

Method	#Params.	Time/q	R@1	R@5	R@10	R@20
NetVLAD [3]	7.23	1.2	4.0	12.4	20.0	30.2
Berton <i>et al.</i> [7]	86.86	1.2	8.0	23.0	33.0	44.7
Orhan <i>et al.</i> [35]	136.62	9830.4	47.0*	66.4*	73.6*	80.3*
PanoVPR (SwinT) _{×8} [41]	28.29	17.0	22.0	42.2	51.8	62.1
Ours -R (SwinT) _{×8}	28.29	1.2	16.8	35.9	46.4	57.3
Ours (SwinT) _{×8}	28.29	3.6	26.6	48.6	58.8	68.3
PanoVPR (SwinT) _{×16} [41]	28.29	48.6	33.6	56.7	66.4	74.4
Ours -R (SwinT) _{×16}	28.29	1.2	17.9	36.5	47.0	59.3
Ours (SwinT) _{×16}	28.29	14.0	32.5	57.2	67.6	74.0
PanoVPR (ConvNeXtS) _{×8} [41]	50.22	17.0	30.9	53.9	64.3	73.9
Ours -R (ConvNeXtS) _{×8}	50.22	1.2	18.3	38.3	49.3	62.2
Ours (ConvNeXtS) _{×8}	50.22	3.6	34.3	59.0	71.1	79.4
PanoVPR (ConvNeXtS) _{×16} [41]	50.22	48.6	40.3	63.0	72.1	80.5
Ours -R (ConvNeXtS) _{×16}	50.22	1.2	19.7	41.7	52.5	64.4
Ours (ConvNeXtS) _{×16}	50.22	14.0	43.4	64.3	73.4	81.2

(b) Performance on the Pitts250K-P2E dataset.

Table 1. Performance comparison on (a) YQ360 and (b) Pitts250K-P2E datasets. ‘-R’ indicates performance without reranking; ‘*’ denotes models trained on an extra-large dataset. The number next to each model indicates the total number of sliding windows (our model: number at the lowest level L). Times (in ms) exclude feature embedding; parameter counts are in millions (M).

5.1. Implementation Details

Training. We use a batch size of 2 for training, and the optimizer is RiemannianAdam [24], which is designed for optimization in hyperbolic space. The learning rate is set to 0.00001, and the margin m of the triplet loss is 0.1. Horizontal flip augmentation is applied during training. We train the model for 60 epochs, with early stopping if performance on the validation set does not improve for 10 consecutive epochs. Following conventional practice [3], we mine 1 hard positive sample and 10 hard negative samples for each query image based on geographical coordinate labels using KNN [42]. During training, we reduced the positive threshold from 25m to 10m. In line with [7], we applied partial mining, using only a portion of the data rather than the entire dataset. For training on the YQ360 [41] dataset, we follow the baseline approach and initialize our model with weights pre-trained on the Pitts250k-P2E dataset [41] before fine-tuning on the YQ360 dataset. For details of datasets and evaluation metric, please refer to the supplementary material (Section S1).

Model setting. All query images are resized to $W, H = 224, 224$, and the database image width is set to $W' = 224 \times 8$. To address the issue of window overlap in database images when $L > 4$, we applied sub-tree partitioning. For details of this technique, please refer to the supplementary material (Section S3). To compare fairly with both P2E and P2P methods, we conducted experiments under two different settings. For comparisons with P2E methods, we followed the baseline protocol and set the descriptor channel dimension $C_d = 768$. For comparisons with P2P methods, we followed their convention and set $C_d = 2048$. For reranking, we used hierarchical levels $\mathbf{h}_d^{(L)}$ across all models presented in the tables, applying the same weights of $w_1 = 0.2$ and $w_L = 0.8$, unless otherwise specified. For the initial prediction, we used $K' = 200$ for the Pitts250k-P2E dataset and $K' = 40$ for the YQ360 dataset.

5.2. Results

Comparison with P2E baselines. Table 1 compares our method with state-of-the-art approaches for P2E VPR on the YQ360 [41] and Pitts250K-P2E datasets [41]. We use the same settings as in PanoVPR [41] for all methods to ensure a fair comparison with P2E baselines.

Our method achieves state-of-the-art performance on both YQ360 (Table 1a) and Pitts250k-P2E (Table 1b), consistently outperforming the sliding window-based baseline PanoVPR [41] across all settings. On YQ360, our model shows higher recall across various backbone architectures and window configurations, while achieving significantly faster retrieval. On Pitts250k-P2E, the speed advantage becomes even more pronounced as the database size increases. Even without reranking, our method achieves competitive performance with sub-millisecond query times (e.g., 0.7ms), and the full model provides the best accuracy-speed trade-off. Although our method performs slightly worse than [35] on Pitts250k-P2E, their approach relies on a substantially larger dataset (7.4M images), more parameters, and an exhaustive sliding window strategy. Qualitative results in Figure 4 also demonstrate that our method is more robust than the P2E baseline. Additional qualitative examples are provided in the supplementary material.

Comparison with P2P baselines and trade-off control. To fairly compare with P2P baselines trained on extra-large datasets, we adopted EigenPlace (ResNet-18 pre-trained on SF-XL [6]) as our backbone and fine-tuned it on Pitts250k-P2E to support hierarchical embedding. Our shared-backbone design allowed seamless integration of the pretrained model for both query and database inputs. We evaluated state-of-the-art P2P methods—SALAD [21], EigenPlace [8], CosPlace [6], and ConvAP [1]—by applying them to panoramic images divided into 16 overlapping crops. As shown in Table 2, our method achieves accuracy comparable to these models while offering substantial

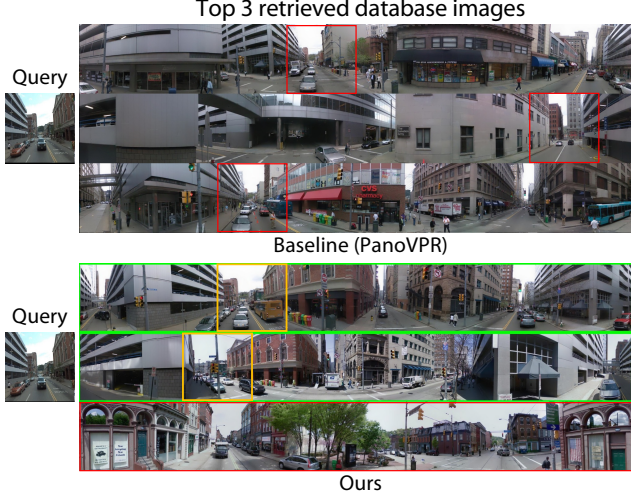


Figure 4. Qualitative results. Correct predictions are outlined in green, while incorrect predictions are outlined in red. In our method, the window with the highest score within the positive pair is highlighted in yellow. Best viewed when zoomed in.

gains in retrieval speed and memory efficiency. We achieve an R@1 of 79.5, comparable to EigenPlace, using $\mathbf{h}_d^{(1)}$ and $\mathbf{h}_d^{(4)}$ with over 8× faster queries and nearly 2× lower storage usage. With $\mathbf{h}_d^{(1)}$ and $\mathbf{h}_d^{(5)}$, we achieve an R@1 of 81.1, surpassing EigenPlace while still maintaining over 5× faster retrieval. Even with only $\mathbf{h}_d^{(1)}$, our model achieves over 100× faster retrieval and requires 20× less storage than SALAD. These results underscore the effectiveness of our hierarchical design in balancing accuracy, speed, and efficiency.

5.3. Ablation studies

We conducted an ablation study to demonstrate the effectiveness of each component of our framework. Our ablations were performed on the Pitts250k-P2E [41] dataset.

Effect of hyperbolic space. We conducted a simple experiment to demonstrate the representational power of hyperbolic space using a Swin-Tiny backbone [30] with an 8-window model. We compared two types of global descriptors: one obtained by applying GeM pooling [37] to all window descriptors in the database image, producing a single Euclidean descriptor, and another created by mapping window descriptors to hyperbolic space and aggregating them via \mathcal{A}_H . This experiment reflects a two-level hierarchical structure, with one level corresponding to a query-sized window and the other to a database-sized window.

As shown in Table 3, even with a simple 2-level hierarchy, the performance of features trained on the hyperbolic space is significantly higher than that of features trained in Euclidean space, justifying our use of hyperbolic space.

Effect of each loss. We analyze the impact of $\mathcal{L}_{\text{hier}}$, \mathcal{L}_{hyp} , and \mathcal{L}_{euc} on model performance using a Swin-Tiny backbone [30] with 8 windows. Table 4 shows the re-

Model	Desc.	R@1	time/q (ms)	Storage (MB)
SALAD [21]	8448	86.8	1196.8	1082.4
EigenPlace [8]	2048	78.3	214.5	262.4
EigenPlace* [8]	2048	80.9	214.5	262.4
CosPlace [6]	2048	73.1	214.5	262.4
ConvAP [1]	2048	72.8	214.5	262.4
Ours -R ($\mathbf{h}_d^{(1)}$ only)*	2048	66.0	10.4	16.4
Ours (Using $\mathbf{h}_d^{(1)}, \mathbf{h}_d^{(4)}$)*	2048	79.5	26.1	147.6
Ours (Using $\mathbf{h}_d^{(1)}, \mathbf{h}_d^{(5)}$)*	2048	81.1	41.8	278.8

Table 2. Comparison on state-of-the-arts P2P VPR methods in new setting. * indicates models fine-tuned on the Pitts250k-P2E.

Feature space	R@1	R@5	R@10	R@20
Euclidean	9.2	20.9	28.6	36.9
Poincaré ball	14.9	30.8	41.9	50.8

Table 3. Performance comparison of a 2-level hierarchy between Euclidean and Hyperbolic feature spaces.

Method	R@1	R@5	R@10	R@20
w/o \mathcal{L}_{euc}	5.2	10.6	15.9	22.0
w/o \mathcal{L}_{hyp}	17.9	36.6	41.7	53.4
w/o $\mathcal{L}_{\text{hier}}$	21.7	41.3	50.2	60.1
Full model	26.6	48.6	58.8	68.3

Table 4. Effect of each loss.

sults when each loss is excluded during training. Removing \mathcal{L}_{euc} significantly degrades the model’s ability to learn robust window-level features, impairing hierarchical learning. Without \mathcal{L}_{hyp} , which supervises query-to-database matching, the model still performs reasonably well, highlighting the strength of the hierarchical structure. Excluding $\mathcal{L}_{\text{hier}}$, which guides hierarchical learning, leads to a performance drop as the model relies only on descriptor matching. These results demonstrate that all three losses play complementary roles, and the full model performs best when they are combined.

6. Conclusions

In this paper, we present HypeVPR, a novel solution for Perspective-to-Equirectangular (P2E) Visual Place Recognition (VPR). HypeVPR leverages the hierarchical structure inherent in equirectangular images through hyperbolic space embeddings, enabling an efficient representation of diverse fields of view (FoVs) within a unified descriptor. This approach supports a multi-scale, coarse-to-fine search strategy that balances global scene context with precise local details. Extensive experiments demonstrate that HypeVPR achieves state-of-the-art performance on various datasets, with significantly faster retrieval speeds. These results highlight HypeVPR’s capability and validate the potential of hyperbolic space for robust P2E VPR. We believe this work encourages further exploration of hyperbolic space within the broader P2E VPR field.

References

- [1] Amar Ali-bey, Brahim Chaib-draa, and Philippe Giguère. Gsv-cities: Toward appropriate supervised visual place recognition. *Neurocomputing*, 513:194–203, 2022. 7, 8
- [2] Amar Ali-bey, Brahim Chaib-draa, and Philippe Giguère. Boq: A place is worth a bag of learnable queries. In *Proceedings of the IEEE/CVF Conference on Computer Vision and Pattern Recognition*, pages 17794–17803, 2024. 2
- [3] Relja Arandjelovic, Petr Gronat, Akihiko Torii, Tomas Padilla, and Josef Sivic. Netvlad: Cnn architecture for weakly supervised place recognition. In *Proceedings of the IEEE conference on computer vision and pattern recognition*, pages 5297–5307, 2016. 1, 7
- [4] Mina Ghadimi Atigh, Julian Schoep, Erman Acar, Nanne Van Noord, and Pascal Mettes. Hyperbolic image segmentation. In *Proceedings of the IEEE/CVF conference on computer vision and pattern recognition*, pages 4453–4462, 2022. 3
- [5] Vassileios Balntas, Edgar Riba, Daniel Ponsa, and Krystian Mikolajczyk. Learning local feature descriptors with triplets and shallow convolutional neural networks. In *Proceedings of the British Machine Vision Conference*, page 3, 2016. 6
- [6] Gabriele Berton, Carlo Masone, and Barbara Caputo. Rethinking visual geo-localization for large-scale applications. In *Proceedings of the IEEE/CVF Conference on Computer Vision and Pattern Recognition*, pages 4878–4888, 2022. 7, 8
- [7] Gabriele Berton, Riccardo Mereu, Gabriele Trivigno, Carlo Masone, Gabriela Csurka, Torsten Sattler, and Barbara Caputo. Deep visual geo-localization benchmark. In *Proceedings of the IEEE/CVF Conference on Computer Vision and Pattern Recognition*, pages 5396–5407, 2022. 1, 7
- [8] Gabriele Berton, Gabriele Trivigno, Barbara Caputo, and Carlo Masone. Eigenplaces: Training viewpoint robust models for visual place recognition. In *Proceedings of the IEEE/CVF International Conference on Computer Vision*, pages 11080–11090, 2023. 7, 8
- [9] Ruiqi Cheng, Kaiwei Wang, Shufei Lin, Weijian Hu, Kailun Yang, Xiao Huang, Huabing Li, Dongming Sun, and Jian Bai. Panoramic annular localizer: Tackling the variation challenges of outdoor localization using panoramic annular images and active deep descriptors. In *2019 IEEE Intelligent Transportation Systems Conference (ITSC)*, pages 920–925. IEEE, 2019. 2
- [10] Myung Jin Choi, Joseph J Lim, Antonio Torralba, and Alan S Willsky. Exploiting hierarchical context on a large database of object categories. In *2010 IEEE computer society conference on computer vision and pattern recognition*, pages 129–136. IEEE, 2010. 1
- [11] Karan Desai, Maximilian Nickel, Tanmay Rajpurohit, Justin Johnson, and Shanmukha Ramakrishna Vedantam. Hyperbolic image-text representations. In *International Conference on Machine Learning*, pages 7694–7731. PMLR, 2023. 2, 3
- [12] Anh-Dzung Doan, Yasir Latif, Tat-Jun Chin, Yu Liu, Thanh-Toan Do, and Ian Reid. Scalable place recognition under appearance change for autonomous driving. In *Proceedings of the IEEE/CVF International Conference on Computer Vision*, pages 9319–9328, 2019. 1
- [13] Aleksandr Ermolov, Leyla Mirvakhabova, Valentin Khrulkov, Nicu Sebe, and Ivan Oseledets. Hyperbolic vision transformers: Combining improvements in metric learning. In *Proceedings of the IEEE/CVF Conference on Computer Vision and Pattern Recognition*, pages 7409–7419, 2022. 3
- [14] Yicheng Fang, Kaiwei Wang, Ruiqi Cheng, and Kailun Yang. Cfv1: A coarse-to-fine vehicle localizer with omnidirectional perception across severe appearance variations. In *2020 IEEE Intelligent Vehicles Symposium (IV)*, pages 1885–1891. IEEE, 2020. 2
- [15] Octavian Ganea, Gary Bécigneul, and Thomas Hofmann. Hyperbolic neural networks. *Advances in neural information processing systems*, 31, 2018. 3
- [16] Zhi Gao, Yuwei Wu, Yunde Jia, and Mehrtash Harandi. Curvature generation in curved spaces for few-shot learning. In *Proceedings of the IEEE/CVF international conference on computer vision*, pages 8691–8700, 2021. 3
- [17] Songwei Ge, Shlok Mishra, Simon Kornblith, Chun-Liang Li, and David Jacobs. Hyperbolic contrastive learning for visual representations beyond objects. In *Proceedings of the IEEE/CVF conference on computer vision and pattern recognition*, pages 6840–6849, 2023. 1, 2, 3
- [18] Christian Häne, Lionel Heng, Gim Hee Lee, Friedrich Fraundorfer, Paul Furgale, Torsten Sattler, and Marc Pollefeys. 3d visual perception for self-driving cars using a multi-camera system: Calibration, mapping, localization, and obstacle detection. *Image and Vision Computing*, 68:14–27, 2017. 1
- [19] Stephen Hausler, Sourav Garg, Ming Xu, Michael Milford, and Tobias Fischer. Patch-netvlad: Multi-scale fusion of locally-global descriptors for place recognition. In *Proceedings of the IEEE/CVF conference on computer vision and pattern recognition*, pages 14141–14152, 2021. 2
- [20] Ziyang Hong, Yvan Petillot, David Lane, Yishu Miao, and Sen Wang. Textplace: Visual place recognition and topological localization through reading scene texts. In *Proceedings of the IEEE/CVF International Conference on Computer Vision*, pages 2861–2870, 2019. 1
- [21] Sergio Izquierdo and Javier Civera. Optimal transport aggregation for visual place recognition. In *Proceedings of the IEEE/CVF Conference on Computer Vision and Pattern Recognition*, pages 17658–17668, 2024. 2, 7, 8
- [22] Valentin Khrulkov, Leyla Mirvakhabova, Evgeniya Ustinova, Ivan Oseledets, and Victor Lempitsky. Hyperbolic image embeddings. In *Proceedings of the IEEE/CVF conference on computer vision and pattern recognition*, pages 6418–6428, 2020. 2, 3, 5
- [23] Sungyeon Kim, Boseung Jeong, and Suha Kwak. Hier: Metric learning beyond class labels via hierarchical regularization. In *Proceedings of the IEEE/CVF Conference on Computer Vision and Pattern Recognition*, pages 19903–19912, 2023. 3
- [24] Max Kochurov, Rasul Karimov, and Serge Kozlukov. Geoopt: Riemannian optimization in pytorch. In *International Conference on Machine Learning*. PMLR, 2020. 7

- [25] Dmitri Krioukov, Fragkiskos Papadopoulos, Maksim Kitsak, Amin Vahdat, and Marián Boguná. Hyperbolic geometry of complex networks. *Physical Review E—Statistical, Nonlinear, and Soft Matter Physics*, 82(3):036106, 2010. 3
- [26] Aditya Kusupati, Gantavya Bhatt, Aniket Rege, Matthew Wallingford, Aditya Sinha, Vivek Ramanujan, William Howard-Snyder, Kaifeng Chen, Sham Kakade, Prateek Jain, et al. Matryoshka representation learning. *Advances in Neural Information Processing Systems*, 35:30233–30249, 2022. 6
- [27] Hyeonjun Kwon, Jinhyun Jang, Jin Kim, Kwonyoung Kim, and Kwanghoon Sohn. Improving visual recognition with hyperbolical visual hierarchy mapping. In *Proceedings of the IEEE/CVF Conference on Computer Vision and Pattern Recognition*, pages 17364–17374, 2024. 3, 6
- [28] Lingxiao Li, Yi Zhang, and Shuhui Wang. The euclidean space is evil: Hyperbolic attribute editing for few-shot image generation. In *Proceedings of the IEEE/CVF international conference on computer vision*, pages 22714–22724, 2023. 3
- [29] Nathan Linial, Avner Magen, and Michael E Saks. Low distortion euclidean embeddings of trees. *Israel Journal of Mathematics*, 106(1):339–348, 1998. 3
- [30] Ze Liu, Yutong Lin, Yue Cao, Han Hu, Yixuan Wei, Zheng Zhang, Stephen Lin, and Baining Guo. Swin transformer: Hierarchical vision transformer using shifted windows. In *Proceedings of the IEEE/CVF international conference on computer vision*, pages 10012–10022, 2021. 8
- [31] Feng Lu, Xiangyuan Lan, Lijun Zhang, Dongmei Jiang, Yaowei Wang, and Chun Yuan. Cricavpr: Cross-image correlation-aware representation learning for visual place recognition. In *Proceedings of the IEEE/CVF Conference on Computer Vision and Pattern Recognition*, pages 16772–16782, 2024. 2
- [32] Sven Middelberg, Torsten Sattler, Ole Untzelmann, and Leif Kobbelt. Scalable 6-dof localization on mobile devices. In *Computer Vision—ECCV 2014: 13th European Conference, Zurich, Switzerland, September 6–12, 2014, Proceedings, Part II* 13, pages 268–283. Springer, 2014. 1
- [33] Maximillian Nickel and Douwe Kiela. Poincaré embeddings for learning hierarchical representations. *Advances in neural information processing systems*, 30, 2017. 3
- [34] Maximillian Nickel and Douwe Kiela. Learning continuous hierarchies in the lorentz model of hyperbolic geometry. In *International conference on machine learning*, pages 3779–3788. PMLR, 2018. 3
- [35] Semih Orhan and Yalın Baştanlar. Efficient search in a panoramic image database for long-term visual localization. In *Proceedings of the IEEE/CVF International Conference on Computer Vision*, pages 1727–1734, 2021. 1, 3, 7
- [36] Devi Parikh and Tsuhan Chen. Hierarchical semantics of objects (hsos). In *2007 IEEE 11th International Conference on Computer Vision*, pages 1–8. IEEE, 2007. 1
- [37] Filip Radenović, Giorgos Tolias, and Ondřej Chum. Fine-tuning cnn image retrieval with no human annotation. *IEEE transactions on pattern analysis and machine intelligence*, 41(7):1655–1668, 2018. 5, 8
- [38] Frederic Sala, Chris De Sa, Albert Gu, and Christopher Ré. Representation tradeoffs for hyperbolic embeddings. In *International conference on machine learning*, pages 4460–4469. PMLR, 2018. 2, 3
- [39] Rik Sarkar. Low distortion delaunay embedding of trees in hyperbolic plane. In *International symposium on graph drawing*, pages 355–366. Springer, 2011. 2, 3
- [40] Yanqing Shen, Sanping Zhou, Jingwen Fu, Ruotong Wang, Shitao Chen, and Nanning Zheng. Structvpr: Distill structural knowledge with weighting samples for visual place recognition. In *Proceedings of the IEEE/CVF Conference on Computer Vision and Pattern Recognition*, pages 11217–11226, 2023. 2
- [41] Ze Shi, Hao Shi, Kailun Yang, Zhe Yin, Yining Lin, and Kaiwei Wang. Panovpr: Towards unified perspective-to-equirectangular visual place recognition via sliding windows across the panoramic view. In *2023 IEEE 26th International Conference on Intelligent Transportation Systems (ITSC)*, pages 1333–1340. IEEE, 2023. 1, 2, 3, 6, 7, 8
- [42] Kashvi Taunk, Sanjukta De, Srishti Verma, and Aleena Sweatapadma. A brief review of nearest neighbor algorithm for learning and classification. In *2019 international conference on intelligent computing and control systems (ICCS)*, pages 1255–1260. IEEE, 2019. 7
- [43] Ruotong Wang, Yanqing Shen, Weiliang Zuo, Sanping Zhou, and Nanning Zheng. Transvpr: Transformer-based place recognition with multi-level attention aggregation. In *Proceedings of the IEEE/CVF Conference on Computer Vision and Pattern Recognition*, pages 13648–13657, 2022. 2
- [44] Tsun-Hsuan Wang, Hung-Jui Huang, Juan-Ting Lin, Chan-Wei Hu, Kuo-Hao Zeng, and Min Sun. Omnidirectional cnn for visual place recognition and navigation. In *2018 IEEE International Conference on Robotics and Automation (ICRA)*, pages 2341–2348. IEEE, 2018. 2
- [45] Zhenzhen Weng, Mehmet Giray Ogut, Shai Limonchik, and Serena Yeung. Unsupervised discovery of the long-tail in instance segmentation using hierarchical self-supervision. In *Proceedings of the IEEE/CVF conference on computer vision and pattern recognition*, pages 2603–2612, 2021. 3
- [46] Sijie Zhu, Linjie Yang, Chen Chen, Mubarak Shah, Xiaohui Shen, and Heng Wang. R2former: Unified retrieval and reranking transformer for place recognition. In *Proceedings of the IEEE/CVF Conference on Computer Vision and Pattern Recognition*, pages 19370–19380, 2023. 2